Published in final edited form as:
Proc SPIE. 2014 March 21; 2014: . doi:10.1117/12.2043145.

Recognizing patterns of visual field loss using unsupervised machine learning

Siamak Yousefi, **Michael H. Goldbaum**, **Linda M. Zangwill**, **Felipe A. Medeiros**, and **Christopher Bowd***
Hamilton Glaucoma Center, Ophthalmology Department, University of California San Diego, 9415 Campus Point Dr, La Jolla, CA, USA 92093

Abstract

Glaucoma is a potentially blinding optic neuropathy that results in a decrease in visual sensitivity. Visual field abnormalities (decreased visual sensitivity on psychophysical tests) are the primary means of glaucoma diagnosis. One form of visual field testing is Frequency Doubling Technology (FDT) that tests sensitivity at 52 points within the visual field. Like other psychophysical tests used in clinical practice, FDT results yield specific patterns of defect indicative of the disease. We used Gaussian Mixture Model with Expectation Maximization (GEM), (EM is used to estimate the model parameters) to automatically separate FDT data into clusters of normal and abnormal eyes. Principal component analysis (PCA) was used to decompose each cluster into different axes (patterns). FDT measurements were obtained from 1,190 eyes with normal FDT results and 786 eyes with abnormal (i.e., glaucomatous) FDT results, recruited from a university-based, longitudinal, multi-center, clinical study on glaucoma. The GEM input was the 52-point FDT threshold sensitivities for all eyes. The optimal GEM model separated the FDT fields into 3 clusters. Cluster 1 contained 94% normal fields (94% specificity) and clusters 2 and 3 combined, contained 77% abnormal fields (77% sensitivity). For clusters 1, 2 and 3 the optimal number of PCA-identified axes were 2, 2 and 5, respectively. GEM with PCA successfully separated FDT fields from healthy and glaucoma eyes and identified familiar glaucomatous patterns of loss.

Keywords

machine learning; unsupervised clustering; pattern recognition; glaucoma; visual field loss

1. INTRODUCTION

Pattern classification is a broad subject with applications in many different fields including biomedicine [1–9]. Recognizing patterns hidden in data sets can result in extracting valuable knowledge about the data. Unsupervised clustering techniques can mathematically describe patterns in data without the use of prior domain knowledge [10–12]. Pattern recognition techniques have been widely used in detecting and monitoring glaucoma [5, 13–15]. Glaucoma is a progressive optic neuropathy eye disease that is the second leading cause of

*cbowd@ucsd.edu.

blindness in the world [16–18]. One of the key aspects of glaucoma management is identifying the disease-related functional defects and monitoring their progression over time. Standard Automated Perimetry (SAP) and Frequency Doubling Technology (FDT) testing are standardized visual field tests that provide information about visual function in the form of sensitivity measurements at 52 different test points (for 24-2 stimuli) across the visual field. The FDT stimulus tests the responses of a subset of all available retinal ganglion cells that have different temporal and spatial summation properties compared to those tested using SAP [19].

Several studies have investigated glaucoma visual field defect patterns [20–23]. Some of these rely just on clinicians and eye experts to subjectively evaluate and recognize the defect patterns [20–23], however, with the advent of new machine learning classifiers, several methods have been proposed based on objective evaluation of large databases of visual fields for recognizing glaucoma patterns using machine learning classifiers [24–27]. One unsupervised learning-based progression detection algorithm, Progression of Patterns (POP), is a recently introduced method based on changing patterns over time using the variational Bayesian independent component analysis mixture model (VIM). However, assessment of FDT visual field defect patterns has not been investigated thoroughly[28].

In the current study we used a Gaussian mixture model [29, 30] and expectation maximization (GEM) approach to separate a set of glaucomatous and normal FDT fields into clusters of glaucomatous and normal results and to determine if this technique can identify axes representing patterns of defect within the glaucoma clusters. We hypothesized that change in GEM defined patterns of defect would perform as well as or better at detecting known glaucomatous change than other techniques that would be evaluated in another study.

2. METHODS

In this section, we first describe the instruments used for data acquisition, the data acquisition and study participants. We then explain the mathematical derivations for modeling the data using GEM. We elaborate the framework and implementation of the glaucoma progression detection hierarchy and the evaluations employed. Next, we describe the clustering step.

2.1 Instruments

Visual field absolute sensitivity was measured at 54 points (2 blind-spot points were excluded) using the 24-2 FDT strategy (Humphrey Matrix, Carl Zeiss Meditec Inc., Dublin, CA) with Welch-Allyn technology (Skaneateles Falls, New York, USA) using the Zippy Estimation by Sequential Testing (ZEST) thresholding algorithm [31, 32].

FDT measures the contrast necessary to detect vertical grating targets that undergo counter-phase flicker. Each target subtends 5 degrees of visual angle and has a spatial frequency of 0.5 cycle/degree and counter phases with a temporal frequency of 18 Hz. The test is based on the frequency-doubling illusion and is a sensitive way to measure glaucomatous visual field loss. Figure 1 shows a sample visual field measurement using a 24-2 FDT system.

2.2 Participants and data acquisition

Individuals included in the current study were participants in the University of California, San Diego (UCSD)-based Diagnostic Innovations in Glaucoma Study (DIGS) and African Descent and Glaucoma Evaluation Study (ADAGES, which also includes participants from University of Alabama, Birmingham, UAB; and New York Eye and Ear Infirmary, NYEE). FDT results from 1,976 eyes of 1,136 individuals were studied.

Each study participant underwent a comprehensive ophthalmologic evaluation, and FDT using the 24-2 test strategy.

2.3 Data modeling using GEM

Assume we have n observations of data and that each observation has d dimensions. To model the given data with a c-component Gaussian mixture model, assume $\boldsymbol{Y} = [Y_1, \ldots, Y_d]^T$ represent the d-dimensional Gaussian random variable and let $\boldsymbol{y} = [y_1, \ldots, y_d]^T$ represent a particular outcome of $\boldsymbol{Y}$. Then, the probability distribution function of c-component finite Gaussian mixture model can be written as [29, 30]

$$p(\boldsymbol{y}|\theta) = \sum_{m=1}^{c} \alpha_m \, p(\boldsymbol{y}|\theta_m) \quad (1)$$

where $\alpha_1, \ldots, \alpha_c$ are weights of each mixing distribution, and each θ_m is the set of parameters defining the m'th mixing distribution component. Therefore, the complete set of model parameters can be written as $\{\theta_1, \ldots, \theta_c, \alpha_1, \ldots, \alpha_c\}$.

Assume the data samples, $\mathcal{Y} = \{\boldsymbol{y}^{(1)}, \ldots, \boldsymbol{y}^{(n)}\}$ are independent and identically distributed. Then we can write the log-likelihood of the c-component Gaussian mixture model as

$$\log p(\mathcal{Y}|\boldsymbol{\theta}) = \log \prod_{i=1}^{n} p(y^{(i)}|\theta_m) = \sum_{i=1}^{n} \log \sum_{m=1}^{c} \alpha_m \, p(\boldsymbol{y}^{(i)}|\theta_m) \quad (2)$$

with constraints on the weighting coefficients as $\alpha_m \geq 0$, $m = 1, \ldots, c$ and $\sum_{m=1}^{c} \alpha_m = 1$.

To find the parameters of this model, we can follow the approach below. The Maximum Likelihood (ML) estimate of the parameters can be written as

$$\hat{\boldsymbol{\theta}}_{ML} = \arg\max \log p(\mathcal{Y}|\boldsymbol{\theta}) \quad (3)$$

Likewise, the Maximum a Posteriori (MAP) framework can be written as

$$\hat{\boldsymbol{\theta}}_{MAP} = \arg\max \{\log p(\mathcal{Y}|\boldsymbol{\theta}) + \log p(\boldsymbol{\theta})\} \quad (4)$$

where $p(\boldsymbol{\theta})$ is the prior on the parameters.

Finding an analytical solution for either ML or MAP is not practical. Therefore, the Expectation Maximization (EM) is the proper solution for computing the parameters in ML or MAP. The local maximum of ML or MAP can be found using EM iteratively. Assume that $\mathbb{Z} = \{\boldsymbol{z}^{(1)}, \ldots, \boldsymbol{z}^{(n)}\}$ indicate which Gaussian mixture component produced each data sample. Therefore, each label is a binary vector $\boldsymbol{z}^{(i)}=[z_1^{(i)}, \ldots, z_c^{(i)}]$, where $z_m^{(i)}=1$ and $z_q^{(i)}=0$, for $q \neq m$, means that the sample $\boldsymbol{y}^{(i)}$ was generated by the mth Gaussian mixture component. Including membership data to the model, we can write

$$\log p(\mathcal{Y}, \mathcal{Z}|\boldsymbol{\theta})=\sum_{i=1}^{n}\sum_{m=1}^{c} z_m^{(i)} \log[\alpha_m p(\boldsymbol{y}^{(i)}|\theta_m)] \quad (5)$$

Then the Expectation step can be written as [33]

$$Q(\theta, \hat{\boldsymbol{\theta}}(t)) \equiv E[\log p(\mathcal{Y}, \mathcal{Z}|\boldsymbol{\theta}|)|\mathcal{Y}, \hat{\boldsymbol{\theta}}(t)]=\log\ p(\mathcal{Y}, \mathcal{W}|\boldsymbol{\theta}) \quad (6)$$

where $\mathcal{W} = E[\ \mathbb{Z}|\ ^{\mathcal{Y}}, \hat{\boldsymbol{\theta}}(t)]$ and $\{t = 0,1,2, \ldots\}$ represents a time sequence.

Since the elements of $\mathbb{Z}$ are binary, we can write

$$w_m^{(i)} \equiv E[z_m^{(i)}|\mathcal{Y}, \hat{\theta}(t)]=\Pr[z_m^{(i)}=1|y^{(i)}, \hat{\theta}(t)]=\frac{\hat{\alpha}_m(t) p\left(\boldsymbol{y}^{(i)}|\hat{\theta}_m(t)\right)}{\sum_{j=1}^{c}\hat{\alpha}_j(t) p\left(\boldsymbol{y}^{(i)}|\hat{\theta}_j(t)\right)} \quad (7)$$

Note that in the case of MAP framework, the maximization step can be written as

$$\hat{\boldsymbol{\theta}}(t+1)=\arg\max\{Q\left(\boldsymbol{\theta}, \hat{\boldsymbol{\theta}}(t)\right)+\log p(\theta)\} \quad (8)$$

The EM algorithm is iterated until a convergence criterion is satisfied. The mathematical framework above was utilized to model the data and perform the clustering.

2.4 Implementation

The GEM data modeling introduced in the previous section essentially combined multivariate Gaussian components to model the visual field data points. Number of samples, n, was 1,976 and the number of dimensions, d, was 53 (52 FDT absolute sensitivity values and participant age). Clusters were assigned by selecting the component that maximized the MAP based on the EM-estimated parameters. Principal component analysis (PCA) was utilized to decompose each cluster into several axes. To identify a globally optimal GEM model that represents glaucoma category and visual field defect patterns, we generated several GEM models and selected a model that provided the best separation of abnormal and normal FDT fields (i.e., best sensitivity and specificity trade off). All stages of the model were implemented in Matlab (Mathworks, Natick, Massachusetts, U.S.A.). True Positives (TP), which are positive instances correctly classified as positive, and False Positives (FP), which are negative instances incorrectly classified as positive, True Negatives (TN), which

are negative instances correctly classified as negatives, and False Negatives (FN), which are positive instances incorrectly classified as negatives were used to define the performance metrics. Specificity, the proportion of all those without disease correctly identified as negative, and sensitivity, proportion of all those with diseases correctly identified as positive comprised the performance metrics.

We assessed the performance of the clustering stage using the reference standard dataset (abnormal and normal FDT visual fields) and the sensitivity/specificity performance metrics defined above.

2.5 Clustering

The absolute visual field sensitivity values from the 52 perimetric locations (54, excluding 2 blind spot locations) and age were used as input to GEM for data modeling. Using the 1,976 DFT visual fields (cross-sectional) as input, GEM modeled *c* categories of glaucoma stages (i.e. *c* clusters) from the data and assigned each of these visual fields to the best fitting cluster. The initiating variable for the learning process was the number of mixing Gaussians, their mean and variance, and the number of clusters, *c*, which ranged from $c = 2–5$. Validation was done after learning the clusters by observing the distribution of abnormal and normal fields in each cluster and the GEM model with nearly 95% specificity and the highest sensitivity was selected from 600 trained GEM models. Figure 3 shows the specificity versus sensitivity for 600 trained GEM models in gray circles and the blue circle is the model selected for pattern generation.

From our assessment of sensitivity-specificity tradeoff among the 600 training GEM models, we found that three clusters provided a better separation of glaucoma and healthy fields. These three clusters were categorized into a normal cluster N, a moderate glaucoma cluster G1 and an advanced glaucoma cluster G2 depending on the centroid of the raw threshold sensitivities of these clusters (normal fields have higher threshold values than glaucomatous fields). In Figure 4, we show 2-D scatterplots of these 53-dimensional clusters for visualization. Figure 4 (left) shows the scatter plot of the superior hemifield (i.e. all visual field locations above the middle horizontal meridian shown in Figure 1) average absolute sensitivity versus the inferior hemifield (all visual field locations below the middle horizontal line as in Figure 1) average absolute sensitivity for all eyes. As can be seen from this figure, the eyes in different clusters are organized from top right to the bottom-left. The clinical interpretation of this organization is discussed in the Results and Discussion sections. Figure 4 (right) shows the scatter plot of MD versus PSD (two global clinical indices of visual function) for all eyes. As can be seen from this figure, three clusters have been organized from high to low MD and PSD values.

3. RECOGNIZING THE GLAUCOMA DEFECT PATTERNS

We decomposed all of the visual fields comprising each cluster into different axes using Principal Component Analysis (PCA). The number of axes in clusters N and G_1 was 2 each, and the number of axes in cluster G_2 was 5. This was determined by assessing the relative contribution of each PCA axis in decomposing the visual fields assigned to the respective

cluster. The visual fields associated with each axis define the patterns of visual defect that we are seeking.

To organize the visual field loss patterns from mild to advanced, the visual field patterns are represented as axes through each cluster centroid. Clinicians typically rely on the Total Deviation (TD) or Pattern Deviation (PD) plots supplied by the instrument software. We used simulated TD plots in our analysis to display the patterns of visual defects in relation to normal eyes. The simulated TD plot is a 52-dimensional vector obtained by subtracting absolute sensitivities at the centroid of the normal cluster N from the absolute sensitivities at the centroid of the glaucomatous clusters and then representing field defects as plots at −2, 0 (cluster centroid), and +2 Standard Deviation (SD) along each of the axes. The numerical TD-like plots were further converted into color representations to aid in visualization. The −26 to +26 values were displayed in equal steps of gray from pure black to pure white.

4. RESULTS

The best GEM model identified 3 clusters. Cluster one, was composed of 1,118 FDT fields within normal limits (94% specificity) and had two axes. Clusters two and three, combined, were composed of 600 abnormal FDT fields (77% sensitivity). Based on evaluation of the average defect within each cluster, cluster two (n=349) was composed of mildly abnormal fields and two axes. Cluster three (n=251) was composed mostly of moderately to severely abnormal fields and 5 axes. FDT fields assigned to an axis resembled both each other and GEM-generated patterns for that axis. Along each axis, pattern severity increased in the positive direction by expansion or deepening of the axis pattern (increased defect area or decreased thresholds in a given area). The visual filed patterns were generated by this model. Figure 5 shows the centroid of the three clusters in the form of deviation from the centroid of the normal cluster. Figure 6 shows the generated patterns across two axes of the normal cluster. All patterns are displayed in −2/2 SD direction of each axis. In Figure 7 we have displayed the glaucoma defect patterns at early stages of the disease across two axes. In Figure 8 we show the identified glaucoma defect patterns across five axes.

5. CONCLUSION

GEM-identified clusters separated normal and abnormal FDT fields with reasonable specificity and sensitivity. In addition, distinctly different and recognizable patterns of glaucomatous field defects were identified. Because GEM is less computationally intensive than other clustering methods, GEM likely is a good candidate as a preliminary process for detecting glaucomatous progression.

References

1. Yousefi S, Kehtarnavaz N, Akins M, Luby-Phelps K, Mahendroo M. Separation of preterm infection model from normal pregnancy in mice using texture analysis of second harmonic generation images. Conf Proc IEEE Eng Med Biol Soc. 2010; 2010:5314–7. [PubMed: 21096067]
2. Yousefi, S.; Kehtarnavaz, N.; Akins, M.; Luby-Phelps, K.; Mahendroo, M. Distinguishing different stages of mouse pregnancy using Second Harmonic Generation images. 42nd Southeastern Symposium on System Theory (SSST); 2010; p. 44-46.

3. Yousefi, S.; Kim, B.; Kehtarnavaz, N. Automating Porosity Features Extraction from Second Harmonic Generation Images of Cervical Tissue. IASTED International Conference on Signal and Image Processing,; 2011.;
4. Xu R, Wunsch DC 2nd. Clustering algorithms in biomedical research: a review. IEEE Rev Biomed Eng. 2010; 3:120–54. [PubMed: 22275205]
5. Goldbaum MH, Sample PA, Zhang Z, Chan K, Hao J, Lee TW, et al. Using unsupervised learning with independent component analysis to identify patterns of glaucomatous visual field defects. Invest Ophthalmol Vis Sci. Oct.2005 46:3676–83. [PubMed: 16186349]
6. Goldbaum MH, Sample PA, White H, Colt B, Raphaelian P, Fechtner RD, et al. Interpretation of automated perimetry for glaucoma by neural network. Invest Ophthalmol Vis Sci. Aug.1994 35:3362–73. [PubMed: 8056511]
7. Suzuki K, Yan P, Wang F, Shen D. Machine learning in medical imaging. Int J Biomed Imaging. 2012; 2012:123727. [PubMed: 22481902]
8. Kononenko I. Machine learning for medical diagnosis: history, state of the art and perspective. Artificial Intelligence in Medicine. 2001; 23:89–109. [PubMed: 11470218]
9. Yousefi S, Goldbaum MH, Balasubramanian M, Jung T-P, Weinreb RN, Medeiros FA, et al. Glaucoma progression detection using structural retinal nerve fiber layer measurements and functional visual field points. IEEE Transactions on Biomedical Engineering. 2014 In press.
10. Katwal SB, Gore JC, Marois R, Rogers BP. Unsupervised spatiotemporal analysis of fMRI data using graph-based visualizations of self-organizing maps. IEEE Trans Biomed Eng. Sep.2013 60:2472–83. [PubMed: 23613020]
11. Zhao Y, Karypis G. Data clustering in life sciences. Mol Biotechnol. Sep.2005 31:55–80. [PubMed: 16118415]
12. Var I. Multivariate data analysis. vectors. 1998; 8:6.
13. Goldbaum MH, Lee I, Jang G, Balasubramanian M, Sample PA, Weinreb RN, et al. Progression of patterns (POP): a machine classifier algorithm to identify glaucoma progression in visual fields. Invest Ophthalmol Vis Sci. Oct.2012 53:6557–67. [PubMed: 22786913]
14. Acharya UR, Dua S, Du X, Sree SV, Chua CK. Automated diagnosis of glaucoma using texture and higher order spectra features. IEEE Trans Inf Technol Biomed. May.2011 15:449–55. [PubMed: 21349793]
15. Hallengren B, Manhem P, Bramnert M, Redlund-Johnell I, Heijl A. Normal visual fields as assessed by computerized static threshold perimetry in patients with untreated primary hypothyroidism. Acta Endocrinol (Copenh). Oct.1989 121:495–500. [PubMed: 2800923]
16. Weinreb RN, Khaw PT. Primary open-angle glaucoma. Lancet. May 22.2004 363:1711–20. [PubMed: 15158634]
17. Kingman S. Glaucoma is second leading cause of blindness globally. Bull World Health Organ. Nov.2004 82:887–8. [PubMed: 15640929]
18. Quigley HA, Broman AT. The number of people with glaucoma worldwide in 2010 and 2020. Br J Ophthalmol. Mar.2006 90:262–7. [PubMed: 16488940]
19. Sample PA, Bosworth CF, Blumenthal EZ, Girkin C, Weinreb RN. Visual function-specific perimetry for indirect comparison of different ganglion cell populations in glaucoma. Invest Ophthalmol Vis Sci. Jun.2000 41:1783–90. [PubMed: 10845599]
20. Alencar LM, Medeiros FA. The role of standard automated perimetry and newer functional methods for glaucoma diagnosis and follow-up. Indian J Ophthalmol. Jan; 2011 59(Suppl):S53–8. [PubMed: 21150035]
21. Rhee K, Kim YY, Nam DH, Jung HR. Comparison of visual field defects between primary open-angle glaucoma and chronic primary angle-closure glaucoma in the early or moderate stage of the disease. Korean J Ophthalmol. Jun.2001 15:27–31. [PubMed: 11530818]
22. Armaly MF. Visual field defects in early open angle glaucoma. Trans Am Ophthalmol Soc. 1971; 69:147–62. [PubMed: 5154258]
23. Drance SM. The early field defects in glaucoma. Invest Ophthalmol. Feb.1969 8:84–91. [PubMed: 5763849]

24. Lau LI, Liu CJ, Chou JC, Hsu WM, Liu JH. Patterns of visual field defects in chronic angle-closure glaucoma with different disease severity. Ophthalmology. Oct.2003 110:1890–4. [PubMed: 14522759]
25. Goldbaum MH, Sample PA, Chan K, Williams J, Lee TW, Blumenthal E, et al. Comparing machine learning classifiers for diagnosing glaucoma from standard automated perimetry. Invest Ophthalmol Vis Sci. Jan.2002 43:162–9. [PubMed: 11773027]
26. Sample PA, Boden C, Zhang Z, Pascual J, Lee TW, Zangwill LM, et al. Unsupervised machine learning with independent component analysis to identify areas of progression in glaucomatous visual fields. Invest Ophthalmol Vis Sci. Oct.2005 46:3684–92. [PubMed: 16186350]
27. Sample PA, Chan K, Boden C, Lee TW, Blumenthal EZ, Weinreb RN, et al. Using unsupervised learning with variational bayesian mixture of factor analysis to identify patterns of glaucomatous visual field defects. Invest Ophthalmol Vis Sci. Aug.2004 45:2596–605. [PubMed: 15277482]
28. Bowd C, Weinreb RN, Lee I, Jang G, Yousefi S, Zangwil LM, et al. Glaucomatous Patterns in Frequency Doubling Technology (FDT) Perimetry Data Identified By Unsupervised Machine Learning Classifiers. PLoS ONE. 2014 In Press.
29. McLachlan, GJ.; Basford, KE. Mixture models: inference and applications to clustering. New York, N.Y: M. Dekker; 1988.
30. McLachlan, GJ.; Peel, D. Finite mixture models. New York: Wiley; 2000.
31. Turpin A, McKendrick AM, Johnson CA, Vingrys AJ. Performance of efficient test procedures for frequency-doubling technology perimetry in normal and glaucomatous eyes. Invest Ophthalmol Vis Sci. Mar.2002 43:709–15. [PubMed: 11867588]
32. Turpin A, McKendrick AM, Johnson CA, Vingrys AJ. Development of efficient threshold strategies for frequency doubling technology perimetry using computer simulation. Invest Ophthalmol Vis Sci. Feb.2002 43:322–31. [PubMed: 11818373]
33. Figueiredo MAT, Jain AK. Unsupervised learning of finite mixture models. IEEE Transactions on Pattern Analysis and Machine Intelligence. Mar.2002 24:381–396.

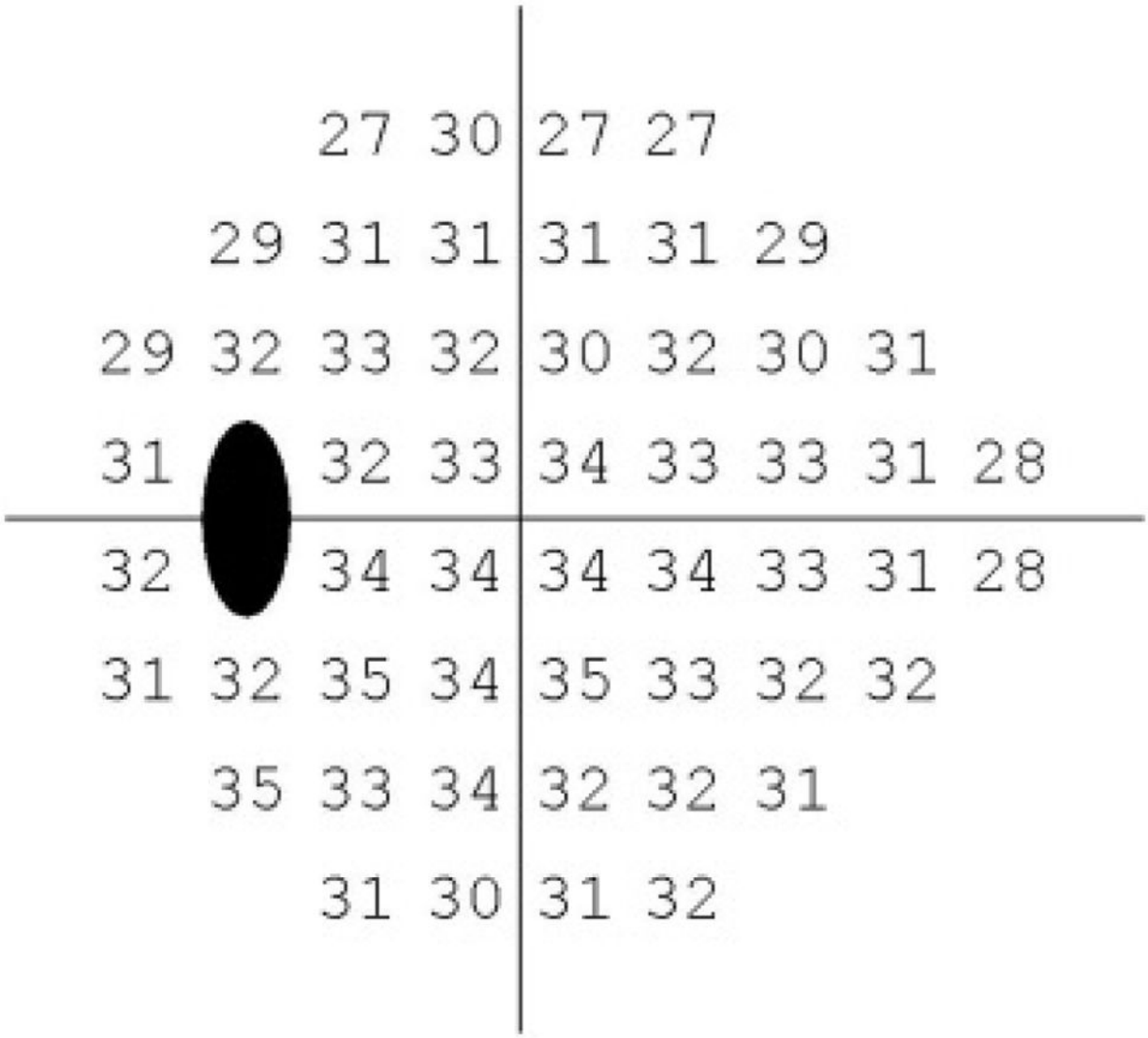

Figure 1.
Absolute threshold sensitivities (in dB) of FDT visual points tested using the 24-2 system.

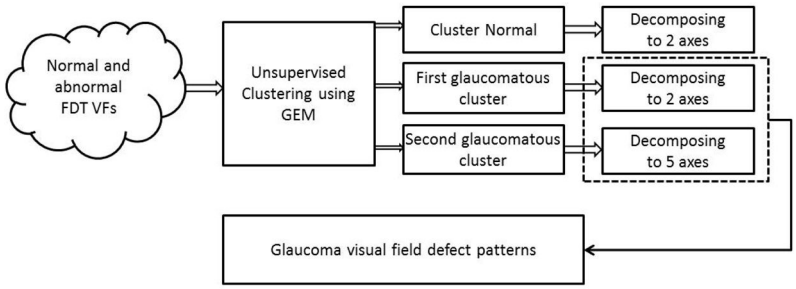

Figure 2.
Block diagram of the clustering method.

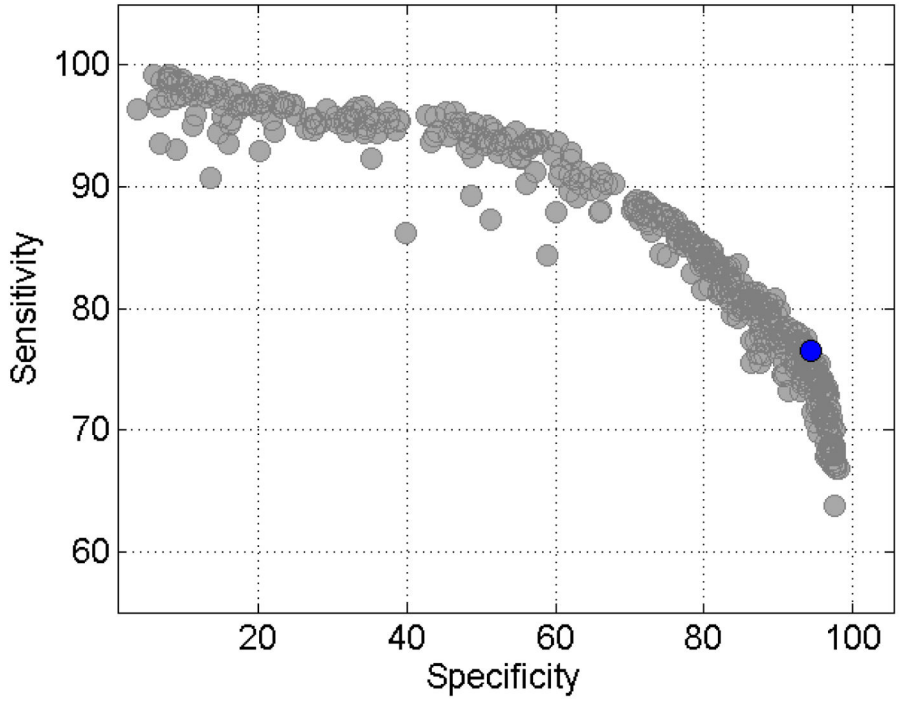

Figure 3.
Performance of all trained GEM models.

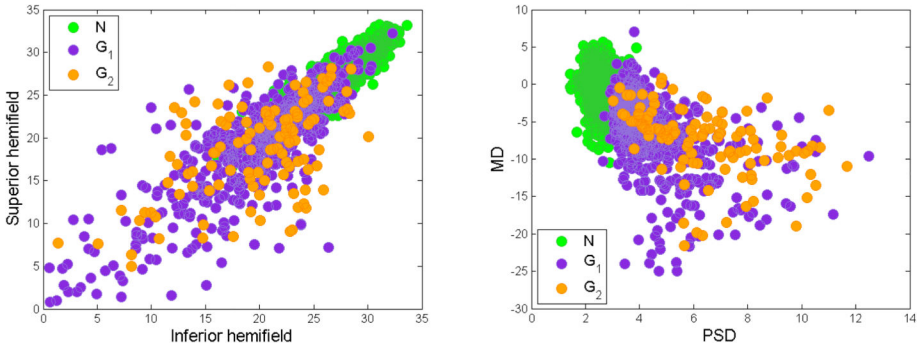

Figure 4.

2-D scatter plot of, left) average of absolute sensitivity values at the superior hemifield versus average of absolute sensitivity values at the inferior hemifield, right) Mean Deviation (MD) versus Pattern Standard Deviation (PSD).

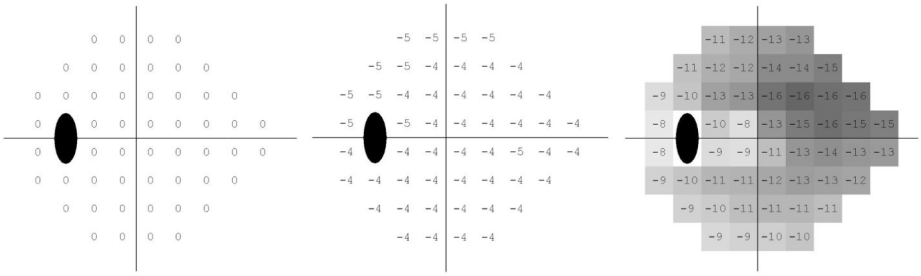

Figure 5.

FDT visual field average defect patters using GEM clustering (The values shown are the total deviation from normal cluster). Left is normal visual field cluster, middle is mild abnormal visual field cluster, and right is moderate to severe abnormal visual field cluster.

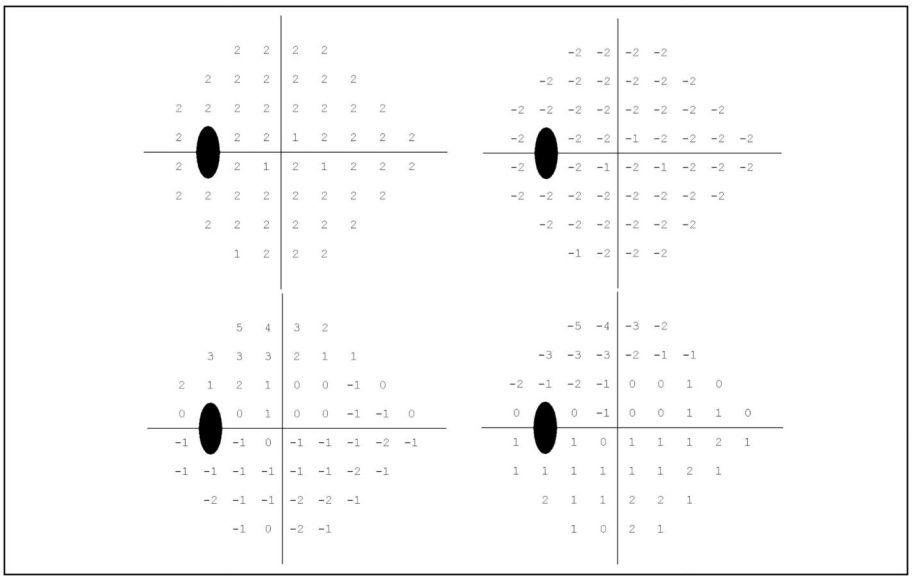

Figure 6.

Normal visual field patterns. Top left: visual field across first axis +2 SD, top right: first axis −2 SD, Bottom left: visual field across second axis +2 SD, Bottom right: visual field across second axis −2 SD.

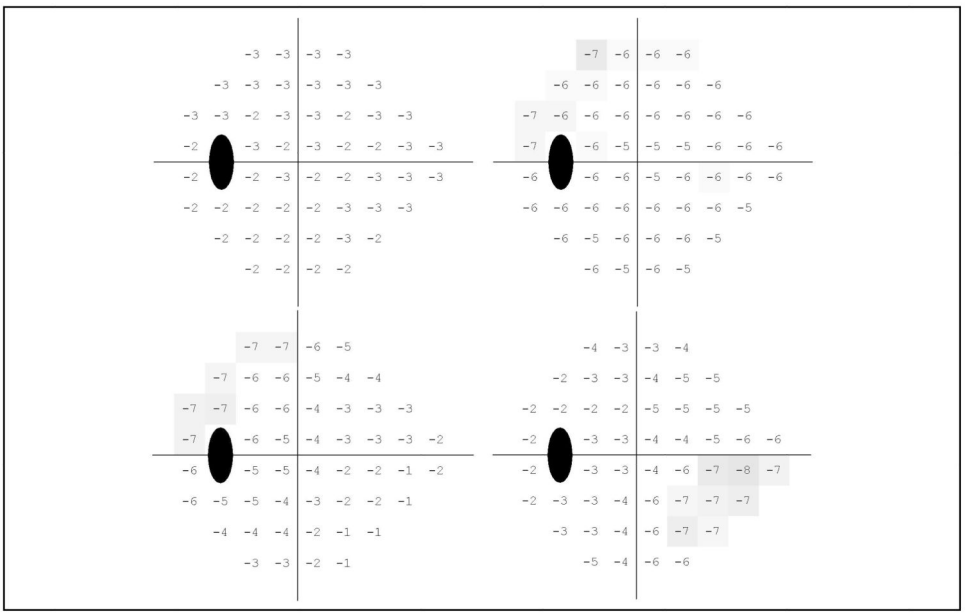

Figure 7.

Early glaucoma visual field patterns. Top left: visual field across first axis +2 SD, top right: first axis −2 SD, Bottom left: visual field across second axis +2 SD, Bottom right: visual field across second axis −2 SD.

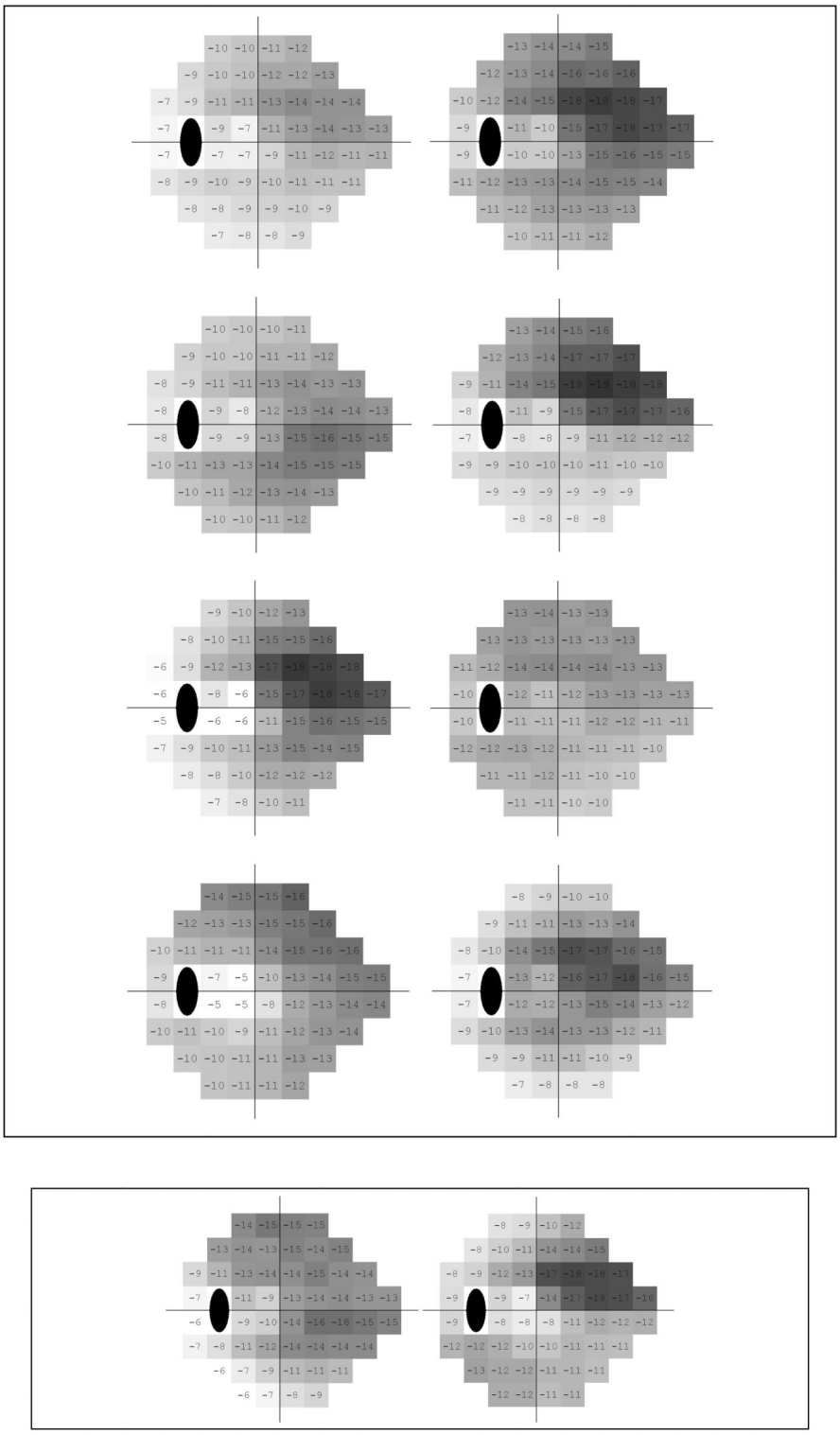

Figure 8.

Moderate to advanced glaucoma visual field patterns. First row left) visual field across first axis +2 SD, first row right) first axis −2 SD, second row left) visual field across second axis

+2 SD, second row right) visual field across second axis −2 SD, third row left) visual field across second axis +2 SD, third row right) visual field across second axis −2 SD, fourth row left) visual field across second axis +2 SD, fourth row right) visual field across second axis −2 SD, fifth row left) visual field across second axis +2 SD, fifth row right) visual field across second axis −2 SD.

Table 1

Demographic information of subjects used.

Parameter	Abnormal visual fields	Normal visual fields	p-value
Number of eyes	786	1190	-
Age at baseline in years (SD)	55.9 (15.3)	50 (14.7)	<0.001
FDT Mean Deviation (MD) in dB (SD)	−5.57 (5.09)	−1.00 (2.80)	<0.001